

RESEARCH

Open Access



Study on the efficacy of amorphous calcium carbonate as a consolidant for calcareous matrix

Wenwen Wang^{1,2}, Shuzhe Wang¹, Qiang Liu¹, Xiaofei Wang¹, Jianfeng Zhu², Hongjie Luo¹ and Shidong Ji^{1*}

Abstract

The popular involvement of amorphous calcium carbonate (ACC) in organisms, usually via a complicated non-classical crystallization pathway, has aroused interest in the scientific community. In recent years, a lot of work has been carried out for the preparation and application of ACC. In this paper, the effectiveness of ACC for the consolidation of calcareous matrix was evaluated. ACC was synthesized through direct carbonation of calcium oxide in ethanol and was introduced into simulated samples as consolidant. A comprehensive study for the assessment of protective effect was carried out by testing surface strength, chromaticity, compressive strength, water vapor permeability, water absorption and freezing–thawing resistance. The results showed that the addition of ACC could significantly improve the surface strength, compressive strength and weatherability of treated samples, while it had only a slight influence on color difference and water vapor permeability. It was confirmed that ACC could connect the loose calcite particles by ‘spot welding’ through heterogeneous nucleation and growth processes. As a consolidant, it demonstrated its merits in this study and could be proposed as an alternative for the protection of weathered calcareous stones.

Keywords: Amorphous calcium carbonate, Amorphous to crystal transformation, Calcareous matrix, Efficacy of consolidation

Introduction

Limestone is a sedimentary rock made of calcium carbonate (CaCO_3), usually in the form of calcite or aragonite. It is abundant in the earth’s crust and has been used as construction and building materials from very ancient times. Many immovable cultural relics, such as stone carvings, monuments, niches and grotto temples, were constructed on the base of limestone. Around the world, especially in Europe, many famous churches were constructed using limestone as the main building material. However, these cultural relics have suffered from damage after long exposure to the natural environment.

To delay further deterioration of these cultural relics bearing fruitful artistic, historic, and scientific information, the most effective way is conducting conservation

and reinforcement. Until now, commonly used materials for the protection of weathered historic calcareous stones include organic consolidant [1–5], inorganic consolidant [6–8] and the hybrid one [9]. Organic consolidant usually possesses nice workability [10], such as good permeability, low viscosity, and exhibit excellent reinforcement performance [11]. However, since the organic materials are apt to be attacked by microorganisms and suffer from thermal-aging and photo-aging, the conservation efficiency of organic polymers has been deeply concerned by the scientific community in this field. While considering the obvious incompatibility with calcareous stones, the shortage of using organic consolidant becomes much clearer. Owing to better physicochemical stability and compatibility than organic consolidant, inorganic material has been considered as an alternative for the consolidation of weathered calcareous stones. Although inorganic consolidant is not easy to breed microorganisms and has good hydrophilicity, its poor permeability and sometimes harmful side-effect caused

*Correspondence: sdki@shu.edu.cn

¹ Institute for the Conservation of Cultural Heritage, Shanghai University, Shanghai 200444, People’s Republic of China
Full list of author information is available at the end of the article

from crystallization and expansion [12] of soluble salts restricted its wild application.

Limewater has been used for a long history. It is widely known that the solubility of calcium hydroxide in water is too low to provide enough consolidant in aqueous phase. Meanwhile, the early stage reinforcement performance [13] of inorganic consolidant is relatively poor. Taking limewater as an example, it needs to absorb CO_2 from air to facilitate carbonation [14] and usually it is a time-consuming process. Attempts had been carried out through adding calcium hydroxide particles and stabilizers in limewater. The breakthrough work was reported by Dei's group [15] for the synthesis of stable nano- $\text{Ca}(\text{OH})_2$ particles in alcohols. It is a well-validated state-of-the-art technology and the effectiveness has been proven in numerous real life conservation cases. The consolidation of calcareous relics by limewater or Nano- $\text{Ca}(\text{OH})_2$ is usually accompanied by the formation of CaCO_3 which is the outcome of carbonation of $\text{Ca}(\text{OH})_2$ [16]. Rodriguez-Navarro et al. [17] revealed that the carbonation of nano-lime in humid air at room temperature involves the initial formation of amorphous calcium carbonate (hereinafter referred to as ACC) and its transformation to metastable vaterite (and minor aragonite) via a dissolution–precipitation process, followed by nonclassical nanoparticle-mediated crystal growth. Subsequently, vaterite (and aragonite) partially dissolves and stable calcite precipitates.

There are several polymorphs of CaCO_3 . The representative crystalline forms include calcite, aragonite and vaterite [18]. Besides these crystal phases, amorphous calcium carbonate also exists and has been found to play a very important role in the formation of many biominerals [19] and also in the initial crystallization stage of biomimetic mineralization. The popular involvement of amorphous calcium carbonate in biological process [19, 20] in organism, usually via a complicated non-classical crystallization pathway [21, 22], has aroused interest in the scientist community. In recent years, a lot of work has been carried out for the preparation and application of ACC.

To date, plenty of methods had been reported for the synthesis of ACC. According to the originating of CO_3^{2-} , they could be categorized to the followings: gas diffusion [23, 24], direct mixing of the aqueous solutions of calcium and carbonate salts [25, 26], hydrolysis of dimethyl carbonate [27], Kitano solution [28] and supplying gaseous CO_2 [29, 30]. A lot of work has been carried out to prepare stable ACC in ethanol media adopting CaCl_2 as the source of calcium [23, 24, 31]. From the view point of conservation, the introducing of chloride ion into ACC may cause the crystallization of soluble salts which are harmful for historic relics [32, 33]. Since ACC prepared

from aqueous solutions usually shows poor stability, so far, most studies involving preparation of stable ACC have introduced organic molecules or inorganic ions to prevent ACC from crystallization. These additives include poly (acrylic acid) [25], carboxyl species [34], magnesium ions [35], phosphorus ions [36], silicate [37] etc.. Recently, Sun et al. [29] reported that high pure ACC could be synthesized by direct carbonation of CaO in methanol, which provided an alternative way for the preparation of phase pure ACC.

The intriguing transformation process from ACC to crystal state still has not been well mastered by scientists until now [18]. In some cases, ACC transfers to crystal state following a traditional ion-by-ion crystal growth pathway, while the non-classical crystal growth pathway [38] was usually reported in other studies. The end product could be presented in multi-crystal powder or even single crystal [39] which depended on the crystallization conditions. In recent years, Rodriguez-Navarro et al. [40] presented the first direct nanoscale evidence showing that faceted calcite crystals could grow non-classically by a layer-by-layer process through the amorphous-to-crystalline transformation and fusion of amorphous calcium carbonate with the underlying calcite substrate.

The novel consolidation approach using ACC prepared by mixing the solutions of $\text{CaCl}_2 \cdot 2\text{H}_2\text{O}$ and Na_2CO_3 was first proposed and tested by A. Burgos Cara et al. [41] in 2017. The authors demonstrated a significant increase in drilling resistance and durability of the treated stone by a dispersion of ACC in isopropanol. In 2021, Pavlakou et al. [42] reported the possible use of ACC for decayed marble. They tested the possibility of treating calcite materials with suspensions of amorphous calcium carbonate (am- CaCO_3 , ACC) and amorphous silica by measuring the rate of dissolution of treated samples in slightly acidic and undersaturated CaCO_3 solutions. Samples deposited with amorphous silica outperformed those treated with ACC. However, the direct use of ACC as a consolidant was still in its very early stage.

From the viewpoint of thermodynamics, ACC is a metastable phase and tends to crystallize spontaneously. Taking advantage of this characteristic of ACC, the main objective of this paper was to explore the possibility of strengthening weathered calcareous matrix by ACC. In this study, a green synthesis process was used by direct carbonation of CaO in alcohol for the formation of ACC. High pure ACC was used as a potential consolidant and its performance was assessed by comprehensive tests.

Materials and methods

Materials

Calcium Oxide (CaO , 98%+), ethanol (high performance liquid chromatography grade, 99.9%) were received from

Adamas-beta and used without further purification. Carbon dioxide (CO₂, 99.995%) was purchased from Air Liquide (Kunshan) Gas Technology Co., Ltd. Commercially available calcium carbonate powder with different grades identified by their particle size (10 mesh, 100 mesh, 400 mesh, 1250 mesh) were purchased from Henan Yixiang New Materials Co., Ltd. and used directly without any pretreatment.

Methods

Synthesis of ACC

The synthesis of ACC was performed according to the previously reported method [29] with some modification by direct carbonation of CaO in ethanol. In a typical procedure, 1.25 g of CaO was added into 100 mL of ethanol, and the slurry was grinded in a planet mill for three hours to disperse it evenly. Then the uniform slurry was transferred to an autoclave. When the temperature reached 50°C, CO₂ was fed into it. The pressure was kept at 0.5 MPa and the reaction continued for 2.5 h under constant stirring at 500 rpm. After the reaction, the pressurized CO₂ was released from the autoclave. To remove the small amount of over grown ACC particles, the reaction mixture was centrifuged at 11,000 rpm for 10 min. An almost hyaline ACC ethanol suspension was acquired after centrifugation.

Characterization of amorphous calcium carbonate

The morphology of ACC was observed by the transmission electron microscope (TEM, JEM-2010, JEOL, Japan) equipped with energy dispersive spectroscopy (EDS). The attachments of high-resolution transmission electron microscopy (HRTEM) image and selected area electron diffraction (SAED) of JEM-2010 were used to get crystallographic information. The crystal structure was investigated by X-ray diffractometry (XRD, D/MAX2200V PCX) using Cu K α radiation ($\lambda=1.5406$ Å), operated under 40 kV and 40 mA. The infrared absorption spectra were determined by a Fourier Transform infrared spectrometer (FTIR, Nicolet IS50). Thermogravimetric (TGA) and differential scanning calorimetry (DSC) analysis were carried out using a Mettler Toledo TGA/DSC

3+ (Schwerzenbach, Switzerland). The TGA/DSC curves were recorded in the temperature range of 25 to 1000 °C in air at a heating rate of 10 °C/min. Viscosity was measured by a rotational viscometer (Smart series, ChemTron Co.) at 25 °C. The particle size of ACC dispersed in ethanol were determined by the Zeta Potentiometer (Zeta sizer Nano).

Preparation and consolidation of simulated samples

Simulated samples were prepared by a similar method suggested by Yang [43] and Zeng et al. [44], which could be considered as a proxy for heavily degraded calcareous stones. Four kinds of calcium carbonate powders (10 mesh, 100 mesh, 400 mesh, and 1250 mesh) were mixed uniformly in the weight ratio of 1:1:1:1. Ethanol was added into the mixture in the ratio of 10 wt.% based on the mass of calcium carbonate powder and then the mixture was homogenized by stirring. The mixture of 10 g or 30 g was weighed for each sample and pressed under 2 MPa or 5 MPa respectively by a tableting machine for preparation of simulated samples. After that, the blocks with the approximate size of $\Phi 20 \times 15$ mm for 10 g powder and $\Phi 50 \times 7$ mm for 30 g powder were obtained.

After drying the test blocks under ambient condition for 24 h, different amounts of ACC were introduced into simulated samples for reinforcement at room temperature. ACC dispersed in ethanol synthesized in “[Synthesis of ACC](#)” section was infiltrated into the simulated samples by spraying. The information about the introduced amount of ACC was shown in Table 1. The amount of ACC introduced by each spray was controlled to be less than 2 wt.% based on the weight of compressed block and the interval between each spray was 24 h. After infiltrating the required amount of ACC, the simulated samples were kept in the environment at room temperature and relative humidity of 70% with different periods before further investigation.

Evaluation of consolidation effect

To evaluate the consolidation effect of ACC on simulated samples, surface strength, chromaticity, simple compression, water vapor permeability, water

Table 1 specification of simulated samples and the information of infiltrated ACC content for each sample

Specification of simulated sample		Infiltrated content of ACC (wt.%) Amount of ACC colloid* (g)					
Size (mm)	Mass* (g)	1wt.%	2wt.%	3wt.%	4wt.%	5wt.%	6wt.%
$\Phi 20 \times 15$	10	3.436	6.873	10.309	13.746	17.182	20.619
$\Phi 50 \times 7$	30	10.309	20.619	30.928	41.237	51.546	61.856

* Errors for the mass of samples and the ACC colloid were ± 0.001 g; the solid content of ACC in ethanol dispersion was 2.91% based on the TGA analysis and corresponding colloid was introduced based on this value.

absorption, and freezing–thawing resistance tests were carried out in this study. Surface strength was determined according to ASTM D3359-09e2. Chromaticity was measured by a I5 desktop spectrophotometer (XRite, USA). The reported chromaticity was the average of the measured values of three individual samples. The color difference, ΔE^* , was calculated by the equation of $\Delta E^* = \sqrt{(\Delta L^*)^2 + (\Delta a^*)^2 + (\Delta b^*)^2}$ (where L^* , a^* and b^* were the measured chromaticity parameters: L^* was brightness, a^* and b^* were chromaticity coordinates (a^* was the red–green parameter and b^* was the blue–yellow parameter)). Compressive strength was measured by a microcomputer controlled electronic universal testing machine (CTM8050) under the loading rate of 0.5 mm/min. Water vapor permeability was determined by a dry test method according to the Chinese national standard of GB/T 17146–2015. A mixture of microcrystalline wax (60 wt.%) and paraffin (40 wt.%) was used as sealing material. The sample with the diameter of 50 mm was used and it was sealed on the top of the test cup. According to that cord, the setup was put in a chamber with the humidity about $50 \pm 3\%$. This configuration provided the high-pressure side of partial water vapor, while the relative humidity of the low-pressure side of partial water vapor was kept at 0% via the absorption of water by anhydrous CaCl_2 loaded in the cup. The temperature was maintained at $23.0 \pm 0.5^\circ\text{C}$ during the test. The freezing–thawing resistance test was conducted according to the Chinese national standard of GB/T 50,266–2013. Before freezing–thawing resistance test, samples were saturated with water by soaking them in water at $15\text{--}20^\circ\text{C}$ for 48 h. One freezing–thawing cycle included the freezing phase (immersing sample in refrigerating fluid at

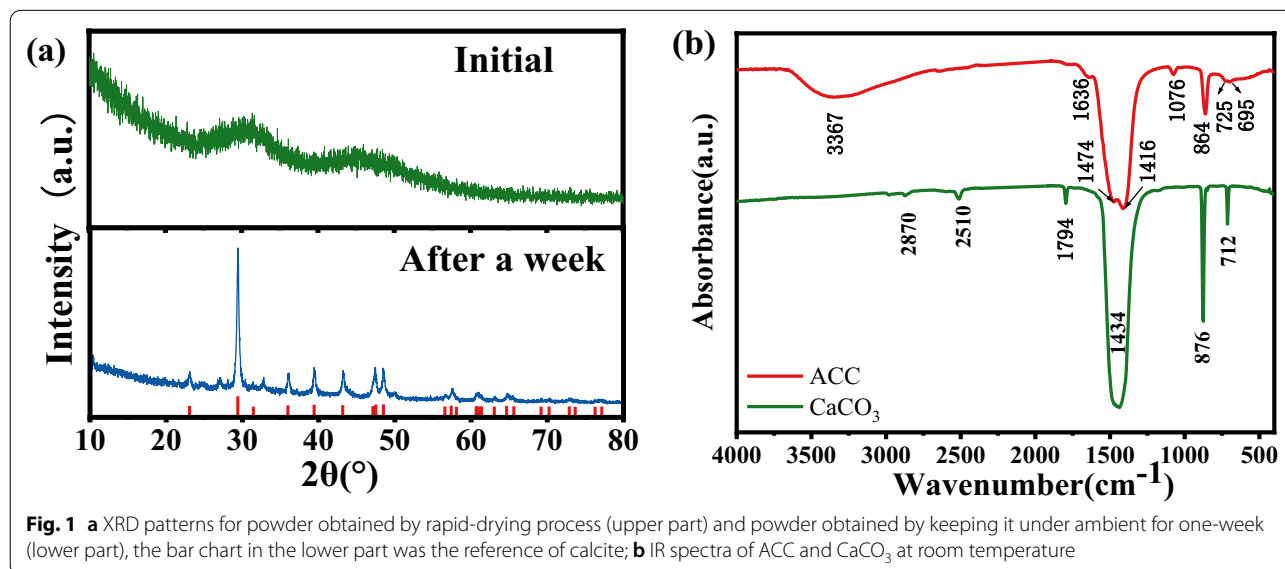
$-20^\circ\text{C} \pm 2^\circ\text{C}$ for four hours) and the following thawing phase (soaking sample in water at $20^\circ\text{C} \pm 2^\circ\text{C}$ for another four hours).

Results and discussion

Characterization of ACC

XRD pattern in the upper part of Fig. 1a showed the crystallinity of the powder obtained by rapid-drying the transparent colloidal suspension synthesized in “Synthesis of ACC” section at 150°C in a pre-heated oven. It presented two broad humps at 30° and 45° respectively, indicating an amorphous phase characteristic [45] of this powder. XRD pattern for powder kept in ambient for a week was also shown in the lower part of Fig. 1a. All peaks could be attributed to the diffraction of calcite, confirming the powder could change from amorphous state to crystal one spontaneously. Samples dried at a lower temperature increasing rate (for example, heating up from room temperature to 150°C in an electric oven by its full power supply) were highly unstable. XRD patterns obtained from samples dried by this process showed it was always the mixture of some sharp peaks and two broad traditional humps. All these results indicated that ACC could nucleate spontaneously from amorphous to crystal state under natural conditions.

The measurement of FT-IR could provide fruitful structure information and it has been performed by many researchers for the characterization of ACC. Figure 1b showed the IR absorption spectra of ACC and calcite at room temperature. The Fourier transform infrared (FT-IR) spectroscopy spectrum of the rapid drying powder showed typical characteristics of an ACC phase. It could be found from the spectra that the characteristic



band ν_4 of calcite at 712 cm^{-1} was replaced by two low-intensity splitting bands at 695 and 725 cm^{-1} , which was a typical feature of ACC [23, 29]. The band at 695 cm^{-1} could be assigned to O–C–O bending (ν_4) in the structure of the amorphous state of CaCO_3 . Bands at 864 and 1076 cm^{-1} could be attributed to out-of-plane bending (ν_2) and symmetric stretch (ν_1) in non-centrosymmetric structures [21]. Compared with the sharp out-of-plane bending (ν_2) at 876 cm^{-1} for calcite, the corresponding one shifted to 864 cm^{-1} and became relatively wider for ACC. In addition, it was worth noting that the infrared spectra of ACC and calcite were quite different in the ν_1 band at 1076 cm^{-1} and the ν_3 band at 1434 cm^{-1} . The absorption peak of ACC at 1076 cm^{-1} was caused by the symmetric stretching vibration of the non-centrosymmetric structure in proto-calcite form. The relative broad absorption peak at 1434 cm^{-1} which could be attributed to the asymmetric stretch of the carbonate ions (ν_3) for calcite separated into two peaks located at 1474 cm^{-1} and 1416 cm^{-1} . The peaks splitting at 712 and 1434 cm^{-1} for calcite were typical characteristics of ACC vibrations [23]. The broad peaks at around 1636 cm^{-1} and the broad band at around 3367 cm^{-1} were due to vibrations of structural water molecules of ACC.

All the above results indicated that ACC was successfully synthesized in our experiment. The electron diffraction (ED) pattern shown in Fig. 2b further confirmed the lack of crystallinity in the sample, as only diffuse diffraction rings were observed. From the TEM image in Fig. 2a, it could be found that ACC tended to form secondary agglomeration particles from nanoparticles with several or several tens' nanometers. The histogram in Fig. 2c unraveled that the particle size distribution of ACC was relatively narrow and centered at 13 nm , which was consistent with the results obtained from TEM observation. The Tyndall effect (Fig. 2d) could be clearly observed in ACC ethanol suspension by an incident light beam, demonstrating a stable dispersed nanoparticle system.

To understand the difference in thermodynamic transformation characteristics between ACC and calcite, the TGA/DSC measurements were carried out. The TGA and DTG (Derivative Thermogravimetry) curves were shown in Fig. 3a, b. The mass drops about 12.38% observed in the TGA curve before $200\text{ }^\circ\text{C}$ were related to physical absorbed and structural water. Considering the preparation conditions and drying process of ACC, the lost water here was the free water absorbed from air during the drying process of liquid samples. In addition, combined with the analysis of TGA and DSC curves, there was an obvious exothermic peak in DSC curve where there was no weight loss at $326\text{ }^\circ\text{C}$ in TGA curve. It indicated that ACC underwent a crystal transformation around this temperature. The exothermic peak could be reasonably explained

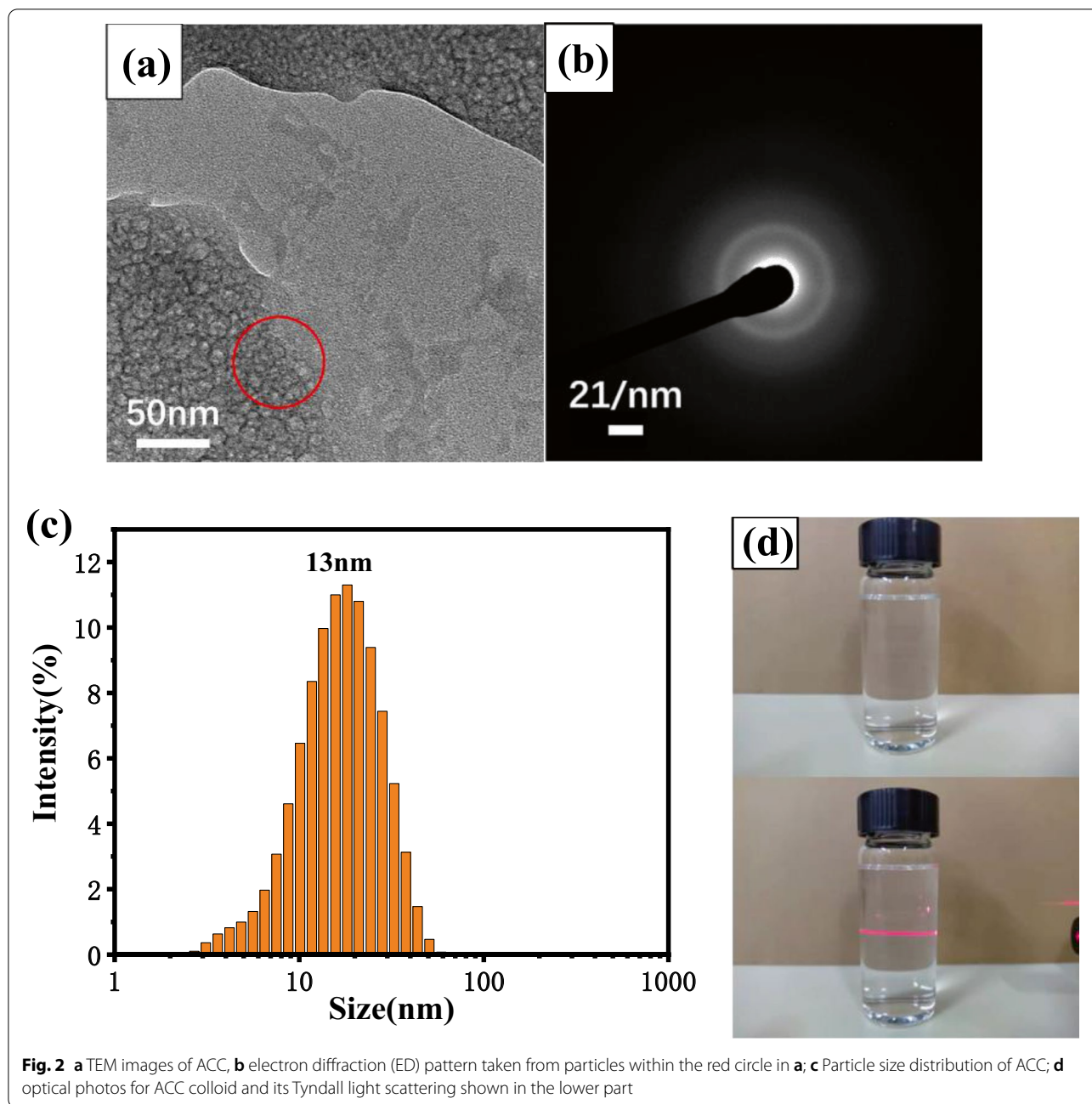
as that high energy state ACC transformed to a lower energy stable state of crystalline calcium carbonate and released the energy of the system.

In addition to the mass drop associated with water, a weight loss above $600\text{ }^\circ\text{C}$ could also be observed on the curves of TGA and DTG. This mass drop was associated with the thermal decomposition of CaCO_3 into CaO. The decomposition of CaCO_3 transformed from ACC shifted to lower temperature compared with that occurred for the reference CaCO_3 powder. The decrease of the decomposition temperature of CaCO_3 could be attributed to the nano-size effect. From the weight loss quantity in the high temperature section, it could be calculated that the CaCO_3 content in ACC was more than $96.9\text{ wt.}\%$ which showed high purity of ACC. Based on the experimental dosage, the solid content of ACC in the colloid after full carbonization of CaO could reach $3.00\text{ wt.}\%$. The calculated value of the solid content of ACC in ethanol dispersion was 2.91% based on the TGA analysis. The decrease of that value was attributed to the removal of a small amount of over grown ACC particles.

Evaluation of the conservation efficiency

Nice workability, one of it was penetration property, could be considered as one major aspect for the fulfillment of conservation. The measured value of viscosity for the obtained colloid was 2.1 cP at $25\text{ }^\circ\text{C}$. Since the ACC prepared in this study had a very small particle size and colloidal suspension had a very low viscosity, its excellent penetration property should be expected. Here, to test the penetration property of ACC in simulated samples, the instantaneous states about a droplet of ACC colloidal suspension from the contact with the simulated sample to completely penetrate into it was visually recorded by high-speed photography. Figure 4 showed the scenarios from 0 – 0.3 s about a droplet of ACC. It's very clear that a drop of ACC suspension could quickly penetrate into the simulated sample, which took less than 0.3 s for the whole process. It illustrated that ACC truly had a good property about penetration which was suitable for further reinforcement of weathered heritage relics.

The surface strength test after the addition of variable amount of ACC to the simulated samples was carried out by the 'Scotch Tape Test' method. The surface strength was evaluated by the calculation of removed mass from the surface of the simulated sample by the scotch tape. The smaller the mass of the removed material from elemental area, the greater the surface strength of the simulated sample. It could be found from Fig. 5a that the surface strength of the simulated sample was significantly improved with the increase of infiltrated ACC content and the effectiveness became tender when the infiltrated amount of ACC exceeded $3\text{ wt.}\%$. The sample treated by

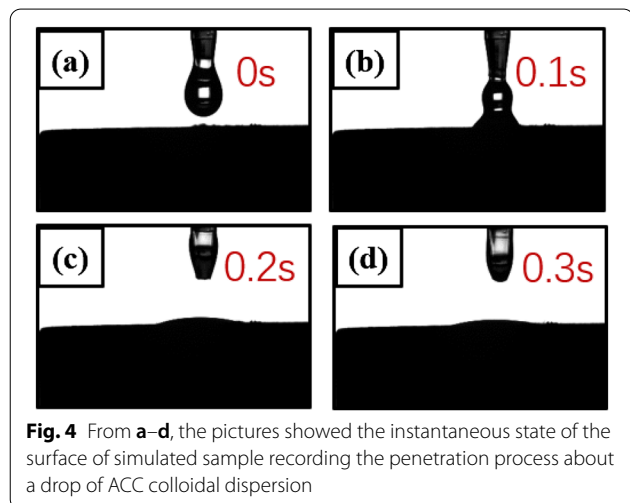
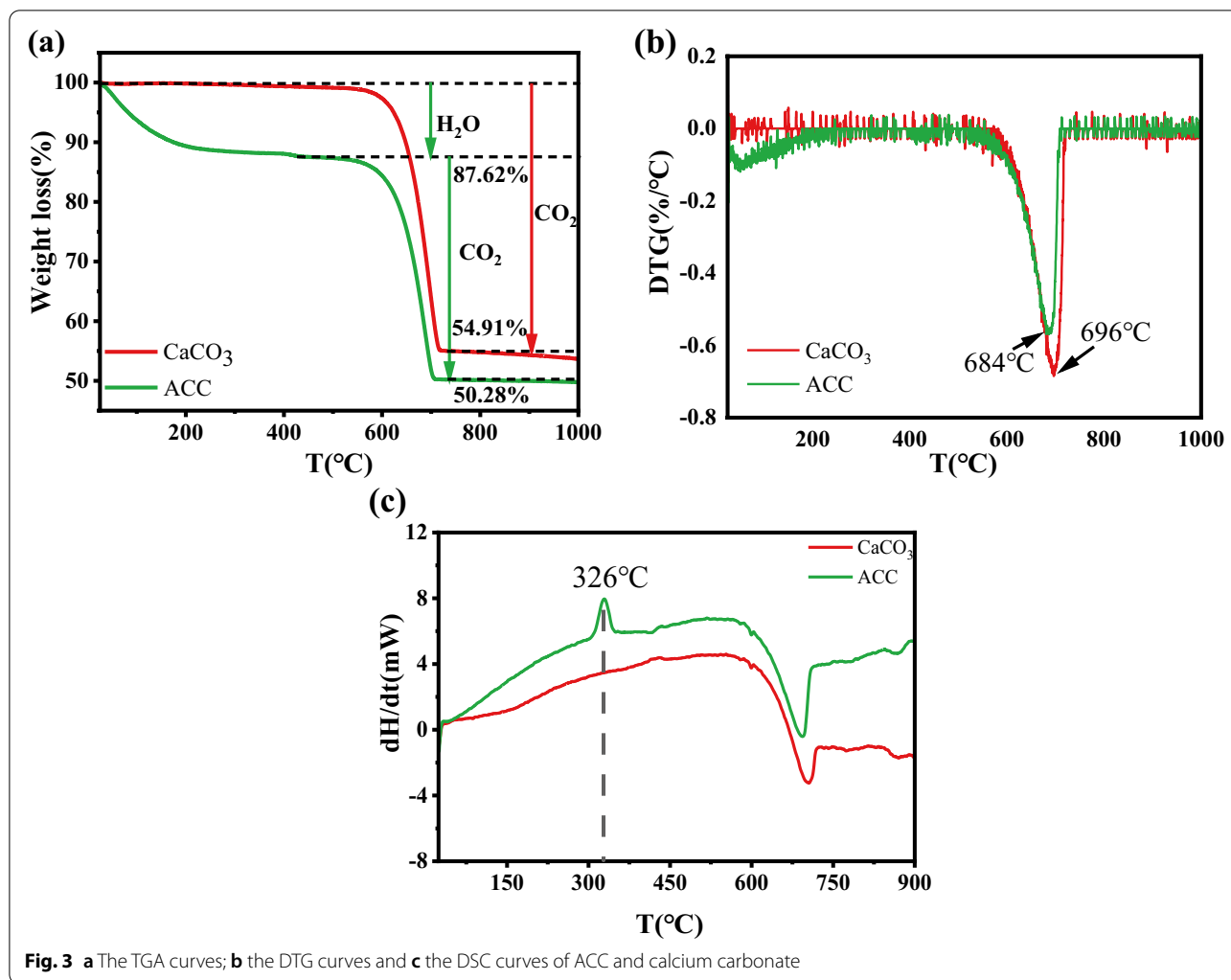


the addition of 6 wt.% ACC showed that the strength was about 13 times higher than that of the blank sample (0 wt.% ACC).

The appearance of samples with different amounts of ACC (1~6 wt.%) were similar with the blank one without the addition of ACC. Here, only chromatic properties of the blank and the samples with the addition of 2 wt.% ACC were listed in Table 2. As comparison, samples with the addition of 2 wt.% GPTMS were also measured. Generally, $\Delta E^* < 5$ is considered to be acceptable for practical

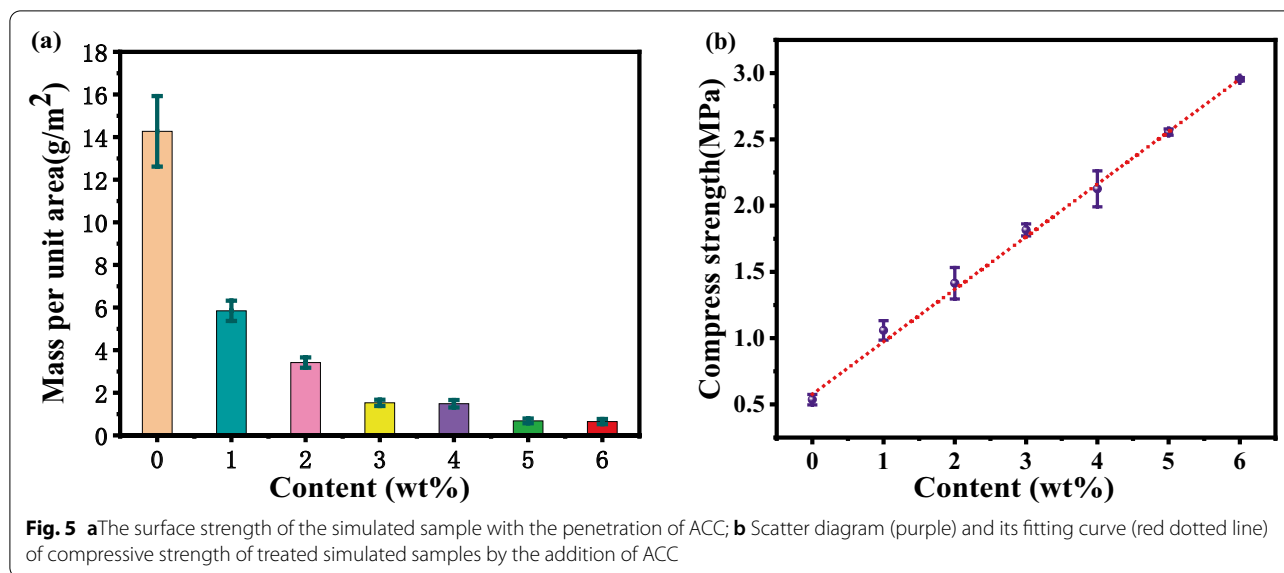
conservation, since such small variation will not be easily detected by naked eyes. In our experiments, the addition of ACC resulted a tiny color change while the addition of 2 wt.% GPTMS made the variation of E^* value exceed this criterion. However, it should be noticed that this result might be different from the consolidation of naturally decayed limestone since the simulated samples were made up of white calcite powder in this study.

To assess the compressive strength of the treated simulated samples, a simple uniaxial compressive test was



performed. It could be speculated from Fig. 5b that as the mass of the infiltrated ACC increased, the compressive strength of the simulated samples increased linearly. The fitting formula was $y = 0.5767 + 0.3964x$, where, “y” represented the compressive strength (MPa) of the simulated sample, and “x” represented the mass ratio of ACC penetrated into the simulated sample.

It could be concluded from our experiments that ACC could be considered as an effective candidate for the reinforcement of weathered calcareous matrix. The introducing of 1wt. % ACC to the simulated sample could double the compressive strength. And the compressive strength had been increased to about 5 folds after introducing ACC with a mass ratio about 6 wt. %. Similar tests were conducted by Yang et al. [43] where nano- $\text{Ca}(\text{OH})_2$ dispersed in Isopropyl alcohol was used as consolidant for comparable simulated samples in our study. In Yang’s work, the introduced nano- $\text{Ca}(\text{OH})_2$ particles transformed into loose rhombohedral crystalline calcite grains

**Table 2** Chromaticity parameters for specific samples

	Blank	2wt% ACC	2wt% GPTMS
L*	92.29	91.73	87.76
a*	0.84	0.94	1.64
b*	3.48	4.22	6.98
ΔE*	–	0.93	5.79

GPTMS 3-Glycidoxypropyltrimethoxysilane

after two weeks' incubation in air. There was no obvious improvement in superficial strength and compressive strength for the simulated weathered stone samples treated with the nano-Ca (OH)₂ dispersion. However, it was very clear that the infiltration of ACC could improve the surface strength and compressive strength of the simulated samples effectively at the same time in our experiments.

The water vapor permeability of samples was tested through the dry method by sealing the simulated sample on the top of the test cup with anhydrous CaCl₂ in it. The water vapor permeability coefficient δ (kg/s·m·Pa) of the measured sample was calculated according to formula (1):

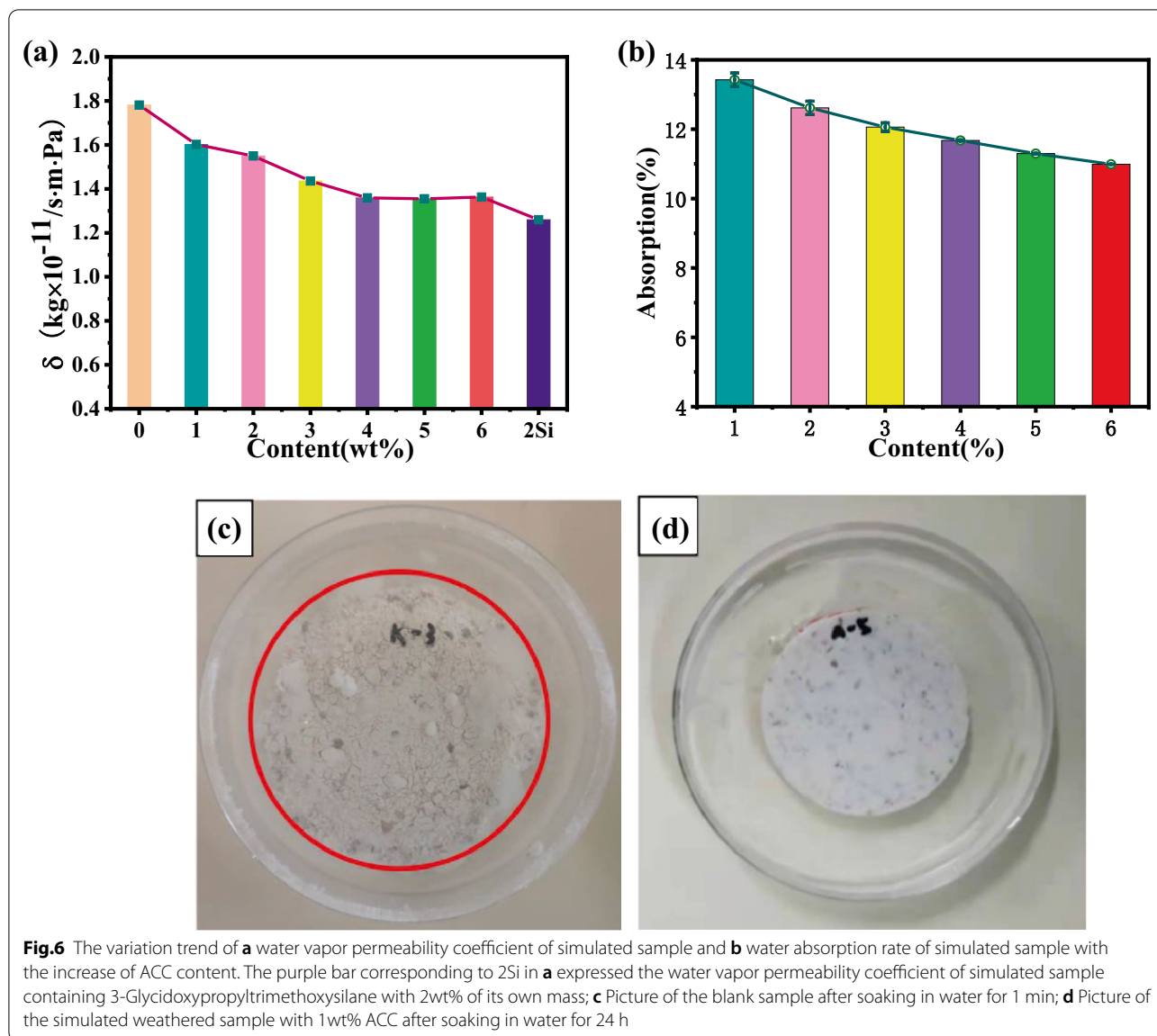
$$\delta = \frac{G}{A \times P_s \times (R_{H1} - R_{H2})} \quad (1)$$

where 'G' represented the wet flow in the unit of kilogram per second (kg/s) through sample, which could be deduced by drawing the curve of the mass increase of the test system with time; 'A' was the exposed area of the tested sample in square meters (m²); P_s was the saturated vapor pressure at the test temperature (23 °C) with the

value of 2.80880 kPa in this experiment; R_{H1} represented the relative humidity (50%) on the high water vapor pressure side; R_{H2} represented the relative humidity (0%) on the low water vapor pressure side.

The results shown in Fig. 6a revealed that the water vapor permeability coefficient did not decrease significantly after adding ACC to the simulated sample. As comparison, the water vapor permeability for sample with the addition of 2 wt.% 3-Glycidoxypropyltrimethoxysilane as a consolidant was also tested. Introducing 2 wt.% of ACC into simulated sample caused a 13% decrease of water vapor permeability, while that value was 33% for sample introduced the same amount of 3-Glycidoxypropyltrimethoxysilane. Since silane had been widely used as consolidant to reinforce weathered stone. Our results indicated that ACC adopted as an additive for the reinforcement of weathered stone showed better performance than silicone-based material [46] in terms of water vapor permeability. And it also suggested that ACC could be considered as a suitable consolidant, since it did not dramatically alter the water vapor permeability. Nowadays, retaining the pathway for water and gas exchange after the addition of conservative materials to heritage relics has aroused deep concern during conservation practice. It has a profound effect on improving the durability of conserved heritage relics, since blocking the pathway for the transportation of salt and water could cause severe damage by the addition of conservation materials [30].

Since water vapor permeability has a close relationship with porosity [47] of the tested sample, the water absorption property of the simulated sample with or without the addition of ACC was tested by recording the mass change



of the simulated sample after 48 h immersing in pure water at room temperature. The value of water absorption for untreated sample could not be obtained since it collapsed completely after immersion in water for only a few minutes. This situation was shown in Fig. 6c. Since there was no cementitious material in the untreated simulated sample, disintegration became inevitable when it was immersed in water. Contrast sharply with the untreated sample destroyed by water rapidly, sample reinforced by the addition of 1wt.% of ACC could maintain intact in water after a long period of immersion. Observation for samples reinforced by the addition of 1~6 wt.% of ACC had lasted for 30 days after being immersed in water and there was no obvious change for these samples. Nice

disintegration resistance performance also confirmed the consolidation efficiency of ACC. It could be found from Fig. 6b that with the increase of the amount of ACC introduced to the samples the water absorption of the simulated sample decreased to some acceptable extent, which was consistent with the results for water vapor permeability. The decrease of water vapor permeability and water absorption were the outcome of the reduction of the volume of pores in the tested samples. It was also an acceptable and reasonable side-effect for the reinforcement of weathered stone by the addition of consolidant especially when the decrease was not severe.

Freezing–thawing resistance experiments were carried out to assess weather resistance of the tested simulated

samples treated by ACC. The number of freezing–thawing cycles for specific simulated sample was counted until obvious cracks appeared in it. The results were shown in Fig. 7. It could be found that the number of anti-freezing–thawing cycles of the simulated sample increased significantly with the increase of the amount of introduced ACC. The number of anti-freezing–thawing cycles increased from 2 to 20 as the content of infiltrated ACC increased from 1 wt.% to 6 wt.%. When 4 wt.% ACC was introduced into the simulated sample, the number of freezing–thawing cycles of the test sample reached 19. Therefore, combined with the results for the study of mechanical strength, it showed that in the process of infiltration reinforcement of simulated sample, the infiltration of 4 wt.% could achieve satisfactory reinforcement effect. At the same time, with the increase of freezing–thawing cycles, the mass of absorbed water in the tested sample increased gradually. It indicated that the freezing–thawing process gradually caused damage

to the tested sample by losing the cementitious material transformed from ACC.

Combining the above experimental results, it could be deduced that the penetration of ACC for the reinforcement of simulated samples was not resulted from a simple particle filling effect in the pores but a cementitious effect on the particles of the tested simulated sample through its own epitaxial growth by nucleation and crystallization or direct transformation by a non-classical pathway. The mechanism will be discussed in detail in the later section. The utility of ACC as a consolidant could not only reinforce the weathered sample effectively but also maintain the water vapor transportation function.

Microstructure analysis and the protective mechanism of ACC for simulated sample

Positive effects for the utility of ACC as a consolidant for calcareous matrix had been revealed clearly in this study. The exhibition of nice performance for the conservation of simulated samples by the addition of ACC should have an inherent relationship with the change of microstructure. To understand this, SEM images corresponding to samples before and after the filtration of ACC were compared. It could be found from the image in Fig. 8a that the edges and surfaces of particles were regular and the boundaries between particles were clear in the untreated sample. When it was reinforced by ACC, the edges and surfaces of particles became irregular and the boundaries between particles became obscure. Some representative spots were highlighted in the red circles in Fig. 8b.

The general impression obtained from the analysis of these SEM images was that the enhancement of mechanical properties for simulated samples was aroused by the fusing of the contacted particles and the filling of powders transformed from ACC. This result could be reasonably explained by heterogeneous nucleation and growth of ACC on the surface of calcareous matrix. The

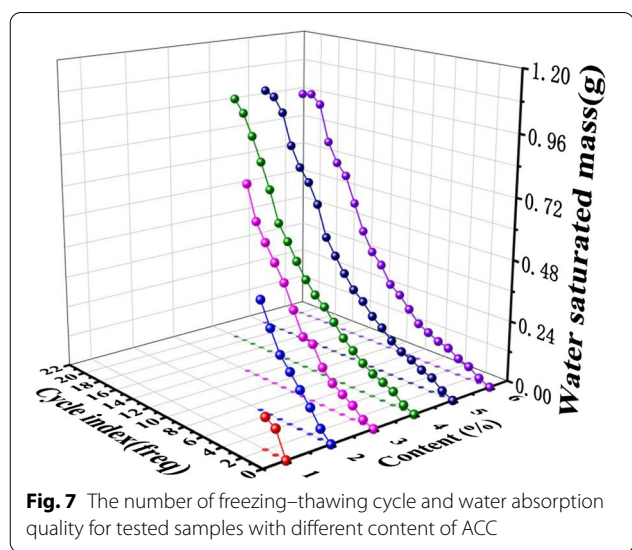


Fig. 7 The number of freezing–thawing cycle and water absorption quality for tested samples with different content of ACC

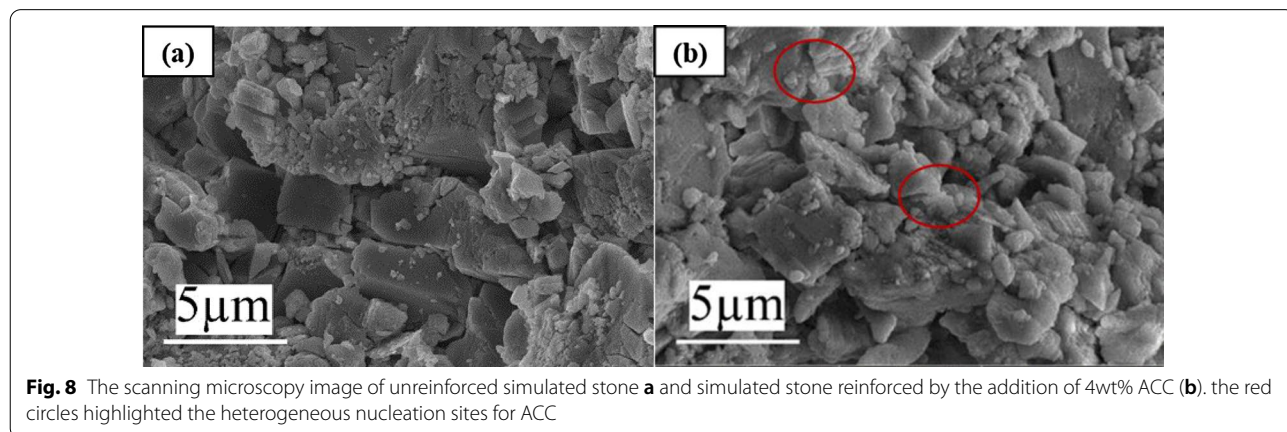


Fig. 8 The scanning microscopy image of unreinforced simulated stone **a** and simulated stone reinforced by the addition of 4wt% ACC **(b)**. the red circles highlighted the heterogeneous nucleation sites for ACC

spontaneous transformation of metastable ACC to stable calcite under nature conditions had been elucidated by many researchers and it was also confirmed in this study. In some cases, the single crystal could also be prepared by this transformation process, when it underwent in well controlled conditions. For example, in the work reported by Tang et al. [30], centimeter-sized monolithic CaCO_3 single crystal could be obtained by the crosslinking of CaCO_3 oligomers using different thermal treatment protocols with careful control of temperature between 300 to 325 °C, or the damaged single-crystalline calcite (Geological Iceland spars was used in their work) could be perfectly repaired using CaCO_3 oligomers.

However, the laboratory-controlled condition was far from that we met when the weathered stone was conserved under natural condition which might cover a wide range of temperature and relative humidity. This study was carried out in a relatively standard condition, which was 25°C and 70% RH. It had been revealed that relative humidity and temperature could result to different consolidation effects when nano- $\text{Ca}(\text{OH})_2$ was used for calcite matrix. For instance, P. López-Arce et al. [48] consolidated dolostone samples used in historical buildings by exposure slaked lime ($\text{Ca}(\text{OH})_2$) nanoparticles at 33 and 75% relative humidity (RH). They found that 75% RH favors the consolidation process by a fast transformation of nano- $\text{Ca}(\text{OH})_2$ into vaterite, monohydrocalcite and calcite and significantly improve the physical and hydric properties of the stones, but do not favor calcite re-crystallization as it occurs at 33% RH. To explore ACC as a consolidant, the impact of temperature and humidity on the evolution of carbonate phases from ACC should be carefully studied in the future.

In our experiments, the synthesized ACC colloid showed low viscosity and high penetration capability. With the volatilization of ethanol, ACC nanoparticles could deposit on the surface of calcite powder. In the process of reinforcement, it was found that a small amount of ACC, such as 4 wt.%, could result in a very good reinforcement effect. Since the calcite transformed from ACC could not be clearly distinguished from the calcareous matrix. The growing habit of calcite spontaneously transformed from metastable ACC colloid was observed on the surface of glass or on the surface of calcite. The morphologies of the resulted calcite were shown in Fig. 9. The calcite functioned as a substrate and it would influence the crystallizing habit of ACC. Under natural conditions without a calcite substrate, it could be found that ACC grew into spherical or short rod-like crystalline CaCO_3 as shown in Fig. 9a. When it grew on the surface of calcite in a confined state, the crystals became very fine and compacted in a closely connected state. These phenomena accorded with the theory of crystal nucleus

formation and growth in crystallography. When the calcite powder was used as substrate, ACC nucleated and transformed into the calcium carbonate crystal and grew on the substrate firstly. After that, the calcium carbonate continuously precipitated in the high-energy surface of the newly formed crystals to reduce the energy of the system and make the nucleation and growth much easier.

Combined with the results in our study, the specific consolidation mechanism of ACC for calcareous matrix was assumed and schematically shown in Fig. 9c. When ACC dispersed in ethanol penetrated into the simulated sample, ACC nanoparticles in colloid quickly adhered to the surface of calcite powder and then the transformation was followed by heterogeneous nucleation and growth. It was assumed that the growth pathway of ACC was similar with that revealed by Rodríguez-Navarro et al. [40] through a nonclassical crystal growth mechanism via the attachment of ACC nanoparticle. The process involved surface diffusion and ultimate incorporation coincided with dehydration and restructuring at macro-steps, deriving from previously attached ACC particles that form 2D islands or macro-spirals on the calcite surface. Since nucleation and growth of calcite from ACC was involved, the kinetics of this process deserved to be further studied. Relative works had been done for the carbonation process of nanolime and the beneficial for future study for ACC system could be forecasted. For example, the 'Boundary Nucleation and Growth' model was adopted by Camerini et al. [49] for the first time to consider the effect of surface area of $\text{Ca}(\text{OH})_2$ nanoparticles on the carbonation kinetics. In their study, the effect of temperature on the carbonation kinetics and on the CaCO_3 polymorphs formation was evaluated.

It should be noticed that the nucleation and growth might happen randomly and continue to grow until the tips of the macro-spirals or islands contacted and fused with the counterpart growing from the adjacent calcite powder. So, the simulated sample was strengthened by 'spot welding' through heterogeneous nucleation and growth pathway of ACC. Obviously, in our experiments we could not assure that all ACC particles were consumed in this effective way. So, to effectively use ACC as consolidant, the method of application and the pretreatment of the substrate deserved to be carefully studied in the future.

Conclusion

Colloid ACC in ethanol was successfully synthesized by direct carbonation of CaO and it was adopted as a consolidant for calcareous matrix taking advantage of its spontaneous transformation from high energy amorphous state to low energy crystal state confined on the surface of calcite powder. The surface strength,

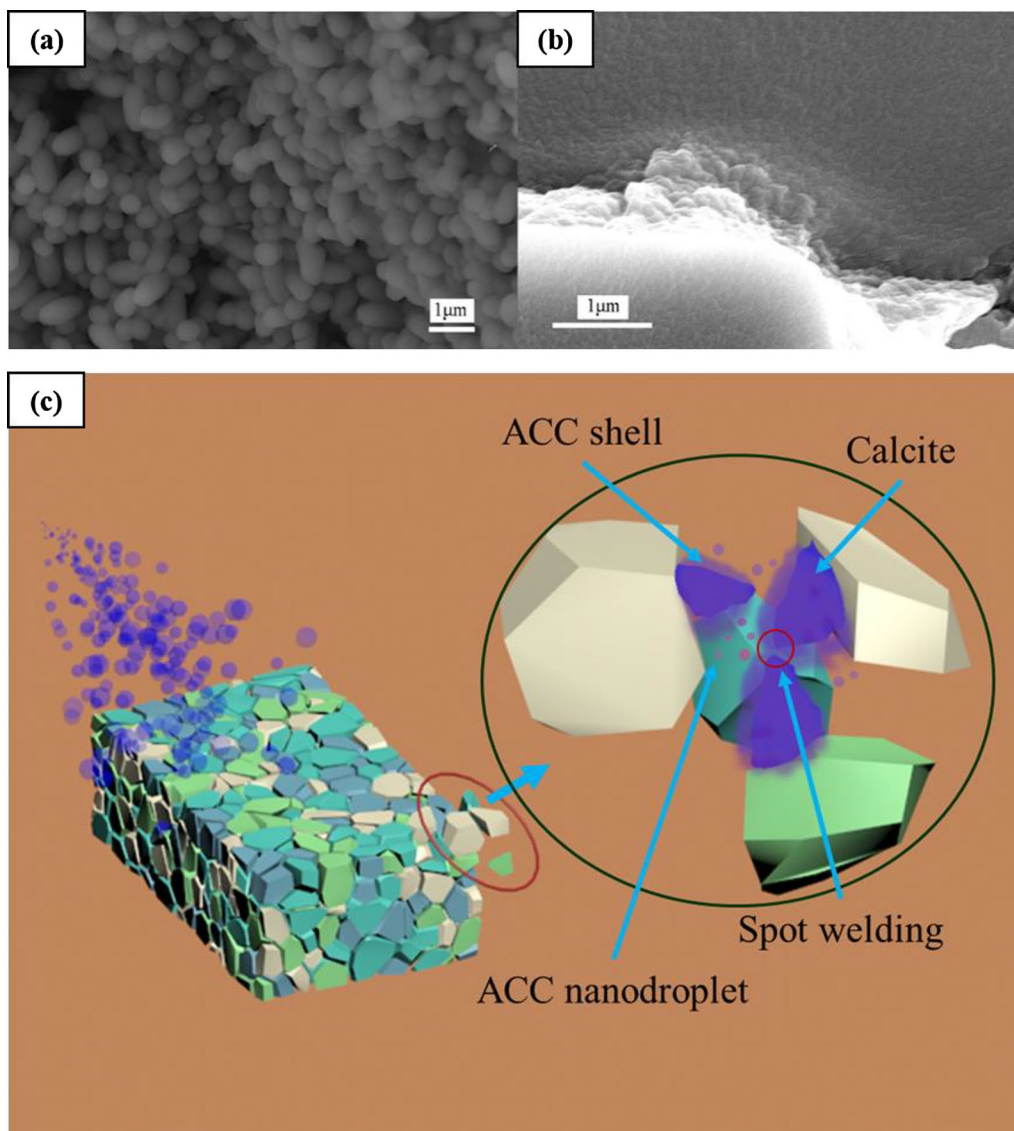


Fig. 9 Morphologies of particles transformed from ACC in natural conditions: on the surface of glass (a); with influence of calcite powder as substrate (b), and the proposed mechanism for the reinforcement of simulated sample by ACC (c)

compressive strength and freezing–thawing resistance of simulated sample could be greatly improved by introducing ACC. Compared with the untreated sample, the compressive strength increased by 5 times and the surface strength increased by 12 times after the addition of 6wt% ACC into the simulated samples. The addition of ACC as consolidant did not change the pore structure significantly, which was reflected by the tender decrease of water vapor permeability coefficient and water absorption rate. The nice conservation performance of ACC could be explained by ‘spot welding’ through heterogeneous nucleation and growth pathway of ACC. Results

about the assessment of conservation efficiency indicated high potential of ACC for the application of the protection for stone cultural relics with calcareous matrix.

Abbreviations

ACC: Amorphous calcium carbonate; TEM: Transmission electron microscope; EDS: Energy dispersive spectroscopy; HRTEM: High-resolution transmission electron microscope; SAED: Selected area electron diffraction; XRD: X-ray diffractometry; FTIR: Fourier transform infrared spectrometer; TGA: Thermogravimetric; DSC: Differential scanning calorimetry; ED: Electron diffraction; DTG: Derivative thermogravimetry.

Acknowledgements

Not applicable.

Author contributions

Conceptualization; SJJ. Methodology and Investigation; WW, SW, QL, XW. Writing—original draft preparation; WW. Writing—review and editing; WW, SW, QL, XW, JZ, HL, SJ. All authors read and approved the final manuscript.

Funding

This study was supported by the National Natural Science Foundation of China (NSFC, No. 52172297) and the National Key R&D Program of China (Project No. 2021YFC1523400; Subject No. 2021YFC1523403).

Availability of data and materials

All data generated or analyzed during this study are included in this manuscript.

Declarations**Competing interests**

The authors declare no conflict of interest.

Author details

¹Institute for the Conservation of Cultural Heritage, Shanghai University, Shanghai 200444, People's Republic of China. ²School of Material Science and Engineering, Shaanxi University of Science & Technology, Shanghai 710021, People's Republic of China.

Received: 29 July 2022 Accepted: 6 October 2022

Published online: 20 October 2022

References

- Franzoni E, Graziani G, Sassoni E. TEOS-based treatments for stone consolidation: acceleration of hydrolysis–condensation reactions by poulticing. *J Sol-Gel Sci Technol*. 2015;74(2):398–405.
- da Fonseca BS, Piçarra S, Pinto AP, de Fátima Montemor M. Development of formulations based on TEOS-dicarboxylic acids for consolidation of carbonate stones. *N J Chem*. 2016;40(9):7493–503.
- Lettieri M, Masieri M, Frigione M. Novel Nano-Filled Coatings for the Protection of Built Heritage Stone Surfaces. *Nanomaterials*. 2021;11(2):301.
- Zhang X, Wen W, Yu H, Qiu F, Chen Q, Yang D. Preparation, characterization of nano-silica/fluoroacrylate material and the application in stone surface conservation. *J Polym Res*. 2016;23(4):75.
- Sbardella F, Pronti L, Santarelli M, AsuaGonzález J, Bracciale M. Waterborne acrylate-based hybrid coatings with enhanced resistance properties on stone surfaces. *Coatings*. 2018;8(8):283.
- Chen W, Zhang Y, Zhang J, Dai P. Consolidation effect of composite materials on earthen sites. *Constr Build Mater*. 2018;187:730–7.
- Chelazzi D, Poggi G, Jaidar Y, Toccafondi N, Giorgi R, Baglioni P. Hydroxide nanoparticles for cultural heritage: consolidation and protection of wall paintings and carbonate materials. *J Colloid Interface Sci*. 2013;392:42–9.
- Rodriguez-Navarro C, Suzuki A, Ruiz-Agudo E. Alcohol dispersions of calcium hydroxide nanoparticles for stone conservation. *Langmuir*. 2013;29(36):11457–70.
- Li D, Xu F, Liu Z, Zhu J, Zhang Q, Shao L. The effect of adding PDMS-OH and silica nanoparticles on sol–gel properties and effectiveness in stone protection. *Appl Surf Sci*. 2013;266:368–74.
- Zielecka M, Bujnowska E. Silicone-containing polymer matrices as protective coatings. *Prog Org Coat*. 2006;55(2):160–7.
- Xu F, Zeng W, Li D. Recent advance in alkoxysilane-based consolidants for stone. *Prog Org Coat*. 2019;127:45–54.
- Michalopoulou A, Maravelaki NP, Stefanis NA, Theoulakis P, Andreou S, Kilikoglou V, Karatasios I. Evaluation of nanolime dispersions for the protection of archaeological clay-based building materials. *Mediterr Archaeol Archaeom*. 2020;20(3):221–42.
- Zullo R, Verdolotti L, Liguori B, Lirer S, de Luna MS, Malara P, Filippone G. Effect of rheology evolution of a sustainable chemical grout, sodium-silicate based, for low pressure grouting in sensitive areas: Urbanized or historical sites. *Constr Build Mater*. 2020;230:117055.
- Wei G, Zhang H, Wang H, Fang S, Zhang B, Yang F. An experimental study on application of sticky rice–lime mortar in conservation of the stone tower in the Xiangji Temple. *Constr Build Mater*. 2012;28(1):624–32.
- Salvadori B, Dei L. Synthesis of Ca(OH)₂ nanoparticles from diols. *Langmuir*. 2001;17:2371–4.
- Silva BA, Ferreira Pinto AP, Gomes A, Candeias A. Effects of natural and accelerated carbonation on the properties of lime-based materials. *J CO₂ Util*. 2021;49:101552.
- Rodriguez-Navarro C, Elert K, Ševčík R. Amorphous and crystalline calcium carbonate phases during carbonation of nanolimes: implications in heritage conservation. *CrystEngComm*. 2016;18(35):6594–607.
- Rimer JD. Inorganic ions regulate amorphous-to-crystal shape preservation in biomineralization. *Proc Natl Acad Sci U S A*. 2020;117(7):3360–2.
- Beniash E, Aizenberg J, Addadi L, Weiner S. Amorphous calcium carbonate transforms into calcite during sea urchin larval spicule growth. *Proc R Soc Lond B Biol Sci*. 1997;264(1380):461–5.
- Politi Y, Arad T, Klein E, Steve Weiner S, Addadi L. Sea urchin spine calcite forms via a transient amorphous calcium carbonate phase. *Science*. 2004;306(5699):1161–4.
- Addadi L, Raz S, Weiner S. Taking advantage of disorder: amorphous calcium carbonate and its roles in biomineralization. *Adv Mater*. 2003;15(12):959–70.
- Jeon T, Na YE, Jang D, Kim IW. Stabilized amorphous calcium carbonate as a precursor of microcoating on calcite. *Materials*. 2020;13(17):3762.
- Chen SF, Colfen H, Antonietti M, Yu SH. Ethanol assisted synthesis of pure and stable amorphous calcium carbonate nanoparticles. *Chem Commun*. 2013;49(83):9564–6.
- Rao C, Guo X, Li M, Sun X, Lian X, Wang H, Gao X, Niu B, Li W. In vitro preparation and characterization of amorphous calcium carbonate nanoparticles for applications in curcumin delivery. *J Mater Sci*. 2019;54(16):11243–53.
- Cai GB, Zhao GX, Wang XK, Yu SH. Synthesis of polyacrylic acid stabilized amorphous calcium carbonate nanoparticles and their application for removal of toxic heavy metal ions in water. *J Phys Chem C*. 2010;114:12948–54.
- Radha AV, Forbes TZ, Killian CE, Gilbert PU, Navrotsky A. Transformation and crystallization energetics of synthetic and biogenic amorphous calcium carbonate. *Proc Natl Acad Sci U S A*. 2010;107(38):16438–43.
- Faatz M, Gröhn F, Wegner G. Amorphous calcium carbonate: synthesis and potential intermediate in biomineralization. *Adv Mater*. 2004;16(12):996–1000.
- Mao L-B, Xue L, Gebauer D, Liu L, Yu X-F, Liu Y-Y, Cölfen H, Yu S-H. Anisotropic nanowire growth via a self-confined amorphous template process: a reconsideration on the role of amorphous calcium carbonate. *Nano Res*. 2016;9(5):1334–45.
- Sun R, Zhang P, Bajnoczi EG, Neagu A, Tai CW, Persson I, Stromme M, Cheung O. Amorphous calcium carbonate constructed from nanoparticle aggregates with unprecedented surface area and mesoporosity. *ACS Appl Mater Interfaces*. 2018;10(25):21556–64.
- Liu Z, Shao C, Jin B, Zhang Z, Zhao Y, Xu X, Tang R. Crosslinking ionic oligomers as conformable precursors to calcium carbonate. *Nature*. 2019;574(7778):394–8.
- Gebauer D, Liu X, Aziz B, Hedin N, Zhao Z. Porous tablets of crystalline calcium carbonate via sintering of amorphous nanoparticles. *CrystEngComm*. 2013;15(6):1257–63.
- Moropoulou A, Kouloumbi N, Haralampopoulos G, Konstanti A, Michailidis P. Criteria and methodology for the evaluation of conservation interventions on treated porous stone susceptible to salt decay. *Prog Org Coat*. 2003;48(2–4):259–70.
- Zhao J, Luo H, Huang X. Migration, distribution, and crystallization of NaCl and Na₂SO₄ solutions in three different media. *Curr Comput-Aided Drug Des*. 2020;10(6):444.
- Sun R, Tai C-W, Strømme M, Cheung O. The effects of additives on the porosity and stability of amorphous calcium carbonate. *Microporous Mesoporous Mater*. 2020;292:109736.
- Shaked H, Polishchuk I, Nagel A, Bekenstein Y, Pokroy B. Long-term stabilized amorphous calcium carbonate—an ink for bio-inspired 3D printing. *Mater Today Bio*. 2021;11: 100120.
- Zou Z, Xie J, Macías-Sánchez E, Fu Z. Nonclassical crystallization of amorphous calcium carbonate in the presence of phosphate ions. *Cryst Growth Des*. 2020;21(1):414–23.

37. Gal A, Weiner S, Addadi L. The stabilizing effect of silicate on biogenic and synthetic amorphous calcium carbonate. *J Am Chem Soc.* 2010;132(38):13208–11.
38. Bruno M. A two-step nucleation model based on diffuse interface theory (DIT) to explain the non-classical view of calcium carbonate polymorph formation. *CrystEngComm.* 2019;21(33):4918–24.
39. Walker JM, Marzec B, Nudelman F. Solid-state transformation of amorphous calcium carbonate to aragonite captured by cryoTEM. *Angew Chem Int Ed Engl.* 2017;56(39):11740–3.
40. Rodriguez-Navarro C, Burgos Cara A, Elert K, Putnis CV, Ruiz-Agudo E. Direct nanoscale imaging reveals the growth of calcite crystals via amorphous nanoparticles. *Cryst Growth Des.* 2016;16(4):1850–60.
41. Burgos-Cara, A. Biomimetic strategies for the consolidation and protection of stone materials used in cultural heritage. Doctoral Thesis, University of Granada, Granada, November 2017.
42. Pavliakou EI, Agraftiotis AG, Tsolaki TG, Lemonia C, Zouvani E, Paraskeva CA, Koutsoukos PG. The protection of building materials of historical monuments with nanoparticle suspensions. *Heritage.* 2021;4(4):3970–86.
43. Yang F, Zhang B, Liu Y, Wei G, Zhang H, Chen W, Xu Z. Biomimetic conservation of weathered calcareous stones by apatite. *New J Chem.* 2011;35(4):887–92.
44. Zeng Y, Zhang B, Liang X. A case study and mechanism investigation of typical mortars used on ancient architecture in China. *Thermochim Acta.* 2008;473:1–6.
45. Gebauer D, Gunawidjaja PN, Ko JY, Bacsik Z, Aziz B, Liu L, Hu Y, Bergstrom L, Tai CW, Sham TK, Eden M, Hedin N. Proto-calcite and proto-vaterite in amorphous calcium carbonates. *Angew Chem Int Ed Engl.* 2010;49(47):8889–91.
46. Rodrigues A, da Fonseca BS, Pinto AF, Piçarra S, Montemor MF. Tailoring alkoxy silanes with poly(ethylene glycol) as potential consolidants for carbonate stones. *Constr Build Mater.* 2021;289:123048.
47. Ban M, Mascha E, Weber J, Rohatsch A, Rodrigues JD. Efficiency and compatibility of selected alkoxy silanes on porous carbonate and silicate stones. *Materials.* 2019;12(1):156.
48. López-Arce P, Gomez-Villalba LS, Pinho L, Fernández-Valle ME, de Buergo MÁ, Fort R. Influence of porosity and relative humidity on consolidation of dolostone with calcium hydroxide nanoparticles: effectiveness assessment with non-destructive techniques. *Mater Charact.* 2010;61(2):168–84.
49. Camerini R, Poggi G, Chelazzi D, Ridi F, Giorgi R, Baglioni P. The carbonation kinetics of calcium hydroxide nanoparticles: A Boundary Nucleation and Growth description. *J Colloid Interface Sci.* 2019;547:370–81.

Publisher's Note

Springer Nature remains neutral with regard to jurisdictional claims in published maps and institutional affiliations.

Submit your manuscript to a SpringerOpen[®] journal and benefit from:

- Convenient online submission
- Rigorous peer review
- Open access: articles freely available online
- High visibility within the field
- Retaining the copyright to your article

Submit your next manuscript at ► [springeropen.com](https://www.springeropen.com)
